Applied Food Research 5 (2025) 100867

Contents lists available at ScienceDirect

Applied Food Research

journal homepage: www.elsevier.com/locate/afres

Effect of catalytic infrared radiation drying parameters on drying kinetics, bioactive compounds, and functional properties of cactus pear cladodes

Néstor Manuel Ortiz-Rodríguez [a], Mayra Denise Herrera [b,*], Jorge A. Zegbe [c,*], Luis Roberto Reveles-Torres [b], Nicolás Iván Román-Roldán [a]

[a] Instituto de Energías Renovables, Universidad Nacional Autónoma de México, Privada Xochicalco s/n, Centro, CP 62580, Temixco, Morelos, Mexico
[b] Campo Experimental Zacatecas, Instituto Nacional de Investigaciones Forestales, Agrícolas y Pecuarias, km 24.5 Carretera Zacatecas-Fresnillo, CP 98500, Calera de Víctor Rosales, Zacatecas, Mexico
[c] Campo Experimental Pabellón, Instituto Nacional de Investigaciones Forestales, Agrícolas y Pecuarias, km 32.5 Carretera Aguascalientes-Zacatecas, CP 20668, Pabellón de Arteaga, Aguascalientes, Mexico

ARTICLE INFO

Keywords:
Antioxidant capacity
Inhibition of digestive enzymes
Modeling
Non-digestible carbohydrates
Opuntia ficus-indica l. mill
Phenolic compounds

ABSTRACT

The influence of catalytic infrared radiation (CIR) on drying characteristics, biocompounds, and functional properties of cactus pear cladode slices (CPCS) was evaluated. Two experiments were conducted. Experiment I varied the LP (liquefied petroleum) gas supply pressure (LPGSP) from 70 to 110 mbar at a 38.0 cm-fixed distance between the emitter and the CPCS. Experiment II varied the distance between CPCS and CIR-emitter at 50 mbar of LPGSP. The Page's model showed the best fit (R^2=0.99) to describe the drying kinetics. In Experiment I, 80 mbar gas supply pressure and 70 min of drying (2615.51 ± 9.65 W/m^2) was the best condition, with higher non-digestible carbohydrates content. Meanwhile, scavenging of ABTS and DPPH were higher at 100 or 110 mbar. In Experiment II, the best distance between CPCS and CIR-emitter was set at 14.0 cm, however, phytochemical losses were observed. Non-digestible carbohydrates, condensed tannins (5.7 mg CAE/g), and saponins (5.0 μg OAE/g) were higher at 24.0 cm, while carotenoids where enhanced at 38.0 cm. Furthermore, 14.0 and 38.0 cm had the highest DPPH and α-amylase, and ABTS and pancreatic lipase inhibition, respectively. The exploratory results establish a foundation for optimization of CIR technology in drying processes, as a promising alternative to reduce drying time while maintaining functional properties, which are essential for human health. Future perspectives include scaling up CIR technology for industrial applications, as it offers significant opportunities to enhance energy efficiency, reduce post-harvest waste, and contribute to food security and sustainability in the agri-food sector.

1. Introduction

Cactus pear (*Opuntia spp*) is a highly valued species cultivated in arid and semi-arid regions worldwide, with Mexico as its genetic diversity center and main producer (Bouazizi et al., 2020). Cladodes, commonly known as cactus pads, are widely used for human and animal consumption due to their high fiber, sugar, mineral, and antioxidant content (Luna-Zapién et al., 2023; Ramírez-Moreno et al., 2013). In the food industry, cactus pear cladodes have been incorporated into various products, including cookies (de Albuquerque et al., 2019), bread, and cakes(Ayadi et al., 2009; Boukid et al., 2015; El-Safy, 2013), demonstrating their versatility as a functional ingredient.

Beyond their nutritional applications, dried cladodes hold significant industrial potential. They have been utilized in corrosion-resistant coatings for steel (Martinez-Molina et al., 2016), as an additive to enhance concrete durability (Torres-Acosta & Díaz-Cruz, 2020), and as a bioadsorbent for wastewater treatment in the textile industry (Barka et al., 2013; Ouhammou et al., 2021). Furthermore, cladodes have been investigated for their bioactive properties in starch-based films for food packaging (FAO, 2015) and as a sustainable feedstock for biofuel production (Kamaraj et al., 2019; Ramírez-Arpide et al., 2019).

Despite their diverse applications, post-harvest losses of cladodes reach up to 53 % in Mexico (FAO, 2015), resulting in significant economic and environmental impacts, including CO_2 emissions (Chen et al., 2020). Drying is a well-established preservation method that extends shelf life while reducing transportation and storage costs (Ladha-Sabur

* Corresponding authors.
E-mail addresses: mayradherrera@gmail.com (M.D. Herrera), zegbe.jorge@inifap.gob.mx (J.A. Zegbe).

https://doi.org/10.1016/j.afres.2025.100867
Received 11 September 2024; Received in revised form 26 February 2025; Accepted 31 March 2025
Available online 2 April 2025

et al., 2019). Conventional drying methods, such as hot air convection drying (HACD), vacuum drying (VD), freeze-drying (FD), and open sun drying (OSD), are commonly employed, but they often suffer from prolonged drying times and high energy consumption (Moses et al., 2014). HACD, the most widely used industrial method, has an efficiency below 50 %, contributing to increased production costs (Tsotsas & Mujumdar, 2011).

Emerging drying technologies, including microwave (MW), radio frequency (RF), and infrared radiation (IR), have demonstrated faster drying kinetics, improved energy efficiency, and better preservation of product quality (Hnin et al., 2019; Zhang et al., 2017). These radiative thermal technologies enable more efficient heating by generating heat directly on the surface or within the moist material, reducing heat losses associated with convective air-drying systems (Ortiz-Rodríguez et al., 2022). Among these, the combination of hot air and infrared radiation (HA-IR) has shown particular promise in reducing drying time and energy consumption (El-Mesery & Mwithiga, 2015; Motevali et al., 2011). Infrared dryers equipped with catalytic infrared (CIR) gas emitters further enhance energy efficiency, reducing energy usage by 60–70 % compared to electric IR and by 20–50 % relative to HACD (Pan & McHugh, 2006). These gas-powered emitters operate within the far-infrared (FIR) range, aligning with the absorption peaks of liquid water, facilitating rapid moisture removal (Krishnamurthy et al., 2008). Unlike electric IR, CIR offers greater operational cost savings, increased durability, and improved adaptability to hybrid drying systems (Das & Das, 2010).

Although extensive research has been conducted on HA-IR drying kinetics and energy efficiency, fewer studies have explored the effects of this technology on phytochemical retention, particularly in cactus pear cladodes (Lee, 2021; Rastogi, 2021). The present study aims to evaluate the impact of combined HA-IR drying using an LP gas CIR emitter on the drying kinetics, bioactive compound retention, and functional properties of *O. ficus-indica* cladode slices. Additionally, mathematical modeling was applied to determine the best-fitting equation for the drying kinetics.

Adjusting drying parameters, particularly LP gas supply pressure and CIR emitter distance, is expected to significantly influence drying kinetics and phytochemical retention. Furthermore, CIR technology has the potential to reduce drying time while preserving or enhancing key nutritional attributes compared to conventional drying methods. This approach offers promising applications for the development of value-added cactus-based products in the food and pharmaceutical industries (Cruz-Rubio et al., 2020).

2. Materials and methods

2.1. Sample preparation

One-year-old 'Roja Lisa' cactus pear cladodes (*O. ficus-indica* L. Mill) were collected from a commercial orchard in Pinos, Zacatecas, Mexico. The cladodes were washed, manually de-spined, and sliced to 5 ± 0.2 mm thickness using a semi-automatic vegetable processor (PV-90, Torrey, Mexico) The initial moisture content was determined with a moisture analyzer (MB45, Ohaus, Switzerland) at 105 °C. The mean mass of the slice samples was 13.9 ± 1.8 g. Drying was conducted until reaching 10 % moisture content (wet basis) to ensure microbiological stability, bioactive compound preservation, and energy efficiency, following previous studies (Amaya-Vélez et al., 2024; Salarikia et al., 2017). After drying, samples were oven-dried (105 °C, 72 h) to determine dry matter and moisture content (wet and dry basis). Finally, samples were ground to 0.5 mm particle size (KRUPS, Germany) and stored at room temperature for subsequent phytochemical analysis.

2.2. CIR dryer description

The efficiency of any CIR-based heating system depends mainly on the type of heat source used. In the CIR emitter, a mixture of LP gas (LPG) and air passes through a platinum catalytic fabric and reacts by oxidation–reduction to produce a controlled bandwidth of IR energy and small amounts of CO_2 and water vapor. In the developed dryer, the gaseous products for combustion were used as a medium to remove the evaporated water during drying, which is equivalent to the convective process with HA. The laboratory-level IR dryer was made up of a CIR emitter model RX 500 operating with LPG (Sunkiss Matherm-Thermoreactor®, Bressolles, France) at 200 V. The IR emission spectrum of the Thermoreactors® is ranging between 2.8 and 10 μm and has a radiant surface of 470 × 470 mm. The emitter has an air fan supplier of catalytic combustion and a thermal resistance to preheat the equipment (Fig. 1A).

The CIR emitter was vertically coupled to a drying chamber lined on its interior walls with anodized aluminum alloys with high reflectivity. The emitter surface temperature and the IR intensity reaching the products are regulated by adjusting the gas supply consumed. In the emitter, the gas supply is regulated by pressure between 50 and 150 mbar, which corresponds to the maximum and the minimum LPG supply, respectively. A perforated stainless-steel tray (450 × 650 mm) platter (3.175 mm in diameter) was installed inside the chamber at a 45° angle (Fig. 1B).

2.3. Instrumentation and monitoring

The operating variables (IR intensity, air temperature, and relative humidity) were simultaneously monitored and recorded in one-min intervals by a data acquisition unit (model 34970A, Agilent®, CA, United States). Air velocity and moisture loss were manually recorded. Room temperature (T) and relative humidity (RH) were recorded simultaneously with a datalogger (Ibérica model PCE-P18, Albacete, Spain). The IR energy intensity on the sample surfaces was measured with a pyrgeometer (CGR4 model, Kipp & Zonen®, Delft, Netherlands) installed on the dome protruded from the drying tray (Fig. 2A). The air velocity between the emitter and the tray was measured with an anemometer (Model 471B, Dwyer, Michigan, United States). Changes in sample slice mass were recorded using a digital scale (model NBL-423, Nimbus®, Kingston, U.K.). The emitter surface temperature (T_1) and the temperature of the hot air generated by the emitter (T_2) were also recorded (Class PT-1000, Mexico City, Mexico). It should be noted that the sensor that records the temperature of the emitter is located outside the catalytic blanket, therefore, it is expected that the temperature of the emitter would be higher. Additionally, temperature of the cladode slice samples during the drying process (T_3) was measured by inserting a PT-1000 sensor equipped with a stainless-steel sheath into one of the slices (Fig. 2A).

2.4. Experimental procedure

The experiments were conducted in the thermosolar plant to dehydrate fresh products (lat. 22° 53N, long. 102° 39W, elevation 2197 m) in Morelos, Zacatecas, Mexico. Before the experiment, the CIR dryer was allowed to run for 45 min for thermal stability. In each test, 250 g of samples were placed. Only the strip of the tray at the level of the pyrgeometer was used. The slices were evenly distributed in a layer on the strip. Two pieces of cladode slices were chosen, one for recording moisture loss and the other for product temperature.

The intensity of the IR energy incident on the product is a critical parameter in CIR drying, as it primarily depends on the distance between the product surface and the IR emitter, as well as the pressure of the LP gas supply. Therefore, the experimental tests were conducted by adjusting the gas pressure between 70 and 110 mbar and placing the samples at three levels with different horizontal distances from the emitter: Level I (14.0 cm), Level II (24.0 cm), and Level III (38.0 cm) (Fig. 2B). The selection of these values was based on preliminary tests, manufacturer specifications, and previous studies. It was observed that

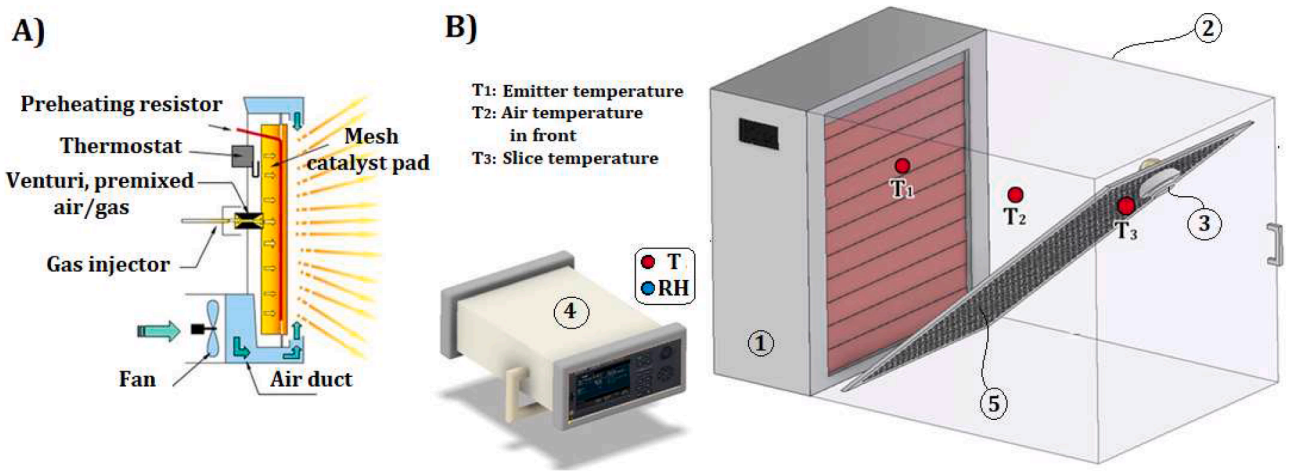

Fig. 1. Components of the CIR emitter adapted from Sunkiss Matherm (2020) (A) and scheme of the CIR dryer instrumented: 1) emitter, 2) drying chamber, 3) pyrgeometer, 4) data acquisition, and 5) perforated tray (B).

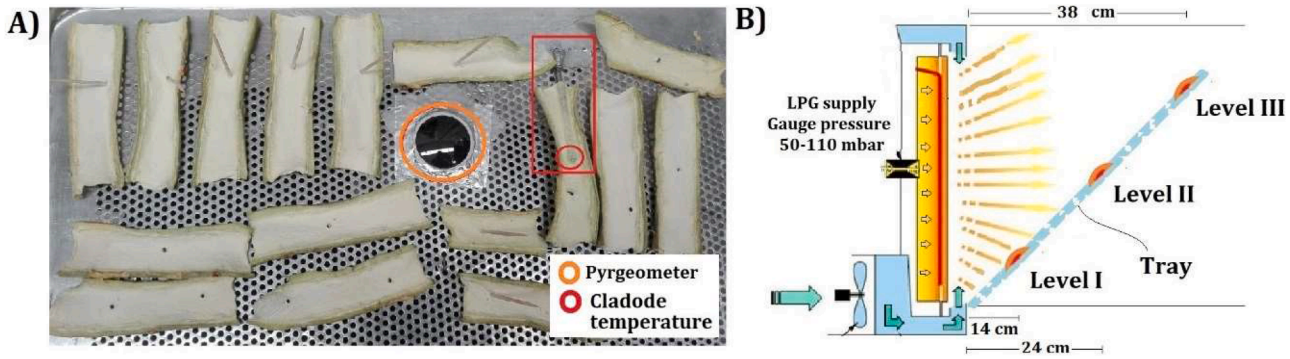

Fig. 2. Arrangement of the cladode slices of 'Roja Lisa' cactus pear on a tray A) and experiment set up for CIR dryer evaluation B).

gas pressures below 70 mbar resulted in insufficient IR radiation, which prolonged drying times and reduced process efficiency. In contrast, pressures above 110 mbar caused overheating and surface charring, particularly at shorter distances (14.0 cm). Similarly, shorter distances combined with higher pressures led to non-uniform drying due to surface overheating. On the other hand, greater distances (38.0 cm) reduced IR energy absorption, which increased drying times. The final selection of parameters also considered the geometric compatibility of the drying chamber. Similar configurations have been reported in previous studies (Motevali et al., 2011; Salarikia et al., 2017). In the present study, two experimental configurations were carried out, replicated three times:

Experiment I. Evaluation of the IR intensity on the cactus cladode slice samples. The distance between the cladode slice surface and the emitter was set at level III and five LP gas pressure supplies were applied from 70 to 110 mbar at 10 mbar intervals.
Experiment II. The effect of the distance between the cladode slice surface and the emitter was evaluated. Cladode slice samples were placed at three distances 14.0 cm (Level I), 24.0 cm (Level II), and 38.0 cm (Level III) and drying was carried out simultaneously. The LP gas supply pressure was set at 50 mbar.

2.5. Drying curve modeling

The evolution curves over time of the moisture content on a dry basis (M_{db}) and wet basis (M_{wb}), were determined from the following equations:

$$M_{db} = \frac{W_s - W_d}{W_d} \quad (1)$$

$$M_{wb} = \frac{W_s - W_d}{W_s} \quad (2)$$

where W_s is the weight of the wet sample (g) and W_d is the weight of the dry sample (g). The drying rate (DR) during the experiments was calculated using Eq. (3)

$$DR = \frac{M_t - M_{t+\Delta t_d}}{\Delta t_d} \quad (3)$$

where DR is (g water/g de dry matter-min), M_t and $M_{t+\Delta t_d}$ are the moisture contents (g/g, d.b.) at t and $t + \Delta t_d$, respectively, and t is the drying time (min). To calculate the moisture ratio (MR), the following equation was used (EL-Mesery et al., 2022):

$$MR = \frac{M_{db}}{M_o} \quad (4)$$

where M_o is the initial moisture content of the sample on a dry basis (g of water/g of dry matter). Thin-layer drying modeling contributes to the understanding of the drying characteristics of agricultural materials. Thus, five mathematical models of thin-layer drying were applied to describe the behavior of HA-IR drying in slices of cactus cladodes over time (Table 1) (Ortiz-Rodríguez et al., 2021). The drying rate constants and coefficients of the drying models were estimated using the Number Cruncher Statistical Systems (NCSS) software (NCSS® Statistical Software, East Kaysville, Utah, USA, 2020).

Table 1
Empirical models applied to drying curves.

Model name	Model equation
Newton	$MR = \exp(-kt)$
Page	$MR = \exp(-kt^n)$
Henderson and Pabis	$MR = a\exp(-kt)$
Logarithmic	$MR = a\exp(-kt) + c$
Midilli–Kucuk	$MR = a\exp(-kt^n) + bt$

a, b, c, coefficients and n, drying exponent specific to each equation; k drying coefficients specific to each equation; t, time.

Statisticians such as the coefficient of determination (R^2) Ec. (5), chi-square (χ^2) Ec. (6) and root mean square error (RMSE) Ec. (7) were used as indicators of the fit of the models tested on the experimental data (Shi et al., 2008).

$$R^2 = 1 - \frac{\sum_{i=1}^{N}\left(MR_{o,i} - MR_{e,i}\right)^2}{\sum_{i=1}^{N}\left(\overline{MR}_o - MR_{e,i}\right)^2} \quad (5)$$

$$\chi^2 = \frac{\sum_{i=1}^{N}\left(MR_{o,i} - MR_{e,i}\right)^2}{N-n} \quad (6)$$

$$RMSE = \sqrt{\frac{1}{N}\sum_{i=1}^{N}\left(MR_{e,i} - MR_{o,i}\right)^2} \quad (7)$$

where $MR_{o,i}$ and $MR_{e,i}$ are the observed and estimated moisture ratios, respectively. $\overline{MR}_o$ is the average experimental moisture ratio. N and n are the number of observations and the number of drying constants, respectively. The highest values of R^2 and the lowest values of RMSE and χ^2 indicate the best ability to estimate the rate of moisture loss during the dehydration of slices of cactus cladodes by HA-IR.

2.6. Phytochemical attributes assessments of cactus cladode slices

2.6.1. Phytochemical analysis

Before phytochemical analysis, dried samples were collected and ground using a domestic grinder (KRUPS, model F2034251, North Rhine-Westphalia, Germany), stored in plastic seal bags, and stored until their analysis, in a fresh environment protecting from direct light exposure.

2.6.2. Non-digestible carbohydrates

The total dietary fiber was determined considering the total dietary fiber assay kit following manual instructions. This commercial kit follows the methodology described by the AOAC, method 985.29. The resistant starch was quantified from the insoluble dietary fiber according to Saura-Calixto et al. (1993), calculated as glucose (mg) x 0.9. The final glucose concentration was quantified by a GOD-PAP kit following kit instructions.

2.6.3. Phenolic compounds

For total phenols, flavonoids, and condensed tannins, extracts were obtained from 1 g of sample mixed with 10 mL of acetone/water/acetic acid (70:29.5:0.5, v/v/v). The mixture was shaken on a digital waving rotator GyroTwister (Labnet International model S1000-B Woodbridge, NJ, USA) for 24 h at room temperature in darkness (Xu & Chang, 2007). The extracts were centrifuged (Centrifuge model 5702R, Eppendorf, Hamburg, Germany) at 4000 rpm for 10 min and the supernatant was collected for further analysis.

Total phenols were quantified by the Folin-Ciocalteu's (FC) reagent solution. Briefly, 40 μL of the acetonic extract was mixed with 460 μL distilled water and 250 μL FC reagent (1:1, v/v) then incubated for 5 min at room temperature. Thereafter, 1250 μL 20 % $NaCO_3$ was added, and the absorbance of samples was read at 765 nm (Multiskan™ GO Microplate Spectrophotometer model 51,119,200, Thermo Scientific™, Waltham, Massachusetts, USA) against a reagent blank. Results were expressed as mg of gallic acid equivalents per gram of dry sample (mg GAE/g) through a calibration curve of the standard with a linearity range of 0 to 0.032 mg/mL (R^2 = 0.99) (Bahammou et al., 2019). Condensed tannins were determined by the vanillin-HCl method; to 50 μL of the acetonic extract, 3 mL of a 4 % methanol vanillin solution and 1.5 mL of concentrated hydrochloric acid were added. The mixture stood for 15 min, and the absorption was read at 500 nm against methanol as a blank. For total flavonoids, 0.25 mL of the extract was mixed with 1.25 mL of distilled water, followed by adding 75 μL of a 5 % $NaNO_2$ solution. After 6 min, 150 μL of a 10 % $AlCl_3$ solution was added. After 5 min, 0.5 mL of NaOH 1 M was added. The absorbance was read at 510 nm. Both determinations were expressed as mg of (+)-catechin equivalents per gram of dry sample (mg CAE/g), using a calibration curve of 0–0.8 mg/mL and 0–0.074 mg/mL (R^2 =0.99), respectively (Xu & Chang, 2007).

2.6.4. Saponins

For total saponins extraction, 0.5 g of samples were mixed with 4 mL of hexane for 6 h, then, centrifuged at 19,000 xg for 5 min. The hexanic phase was recovered and evaporated to dryness at 70 °C in a water bath (Lab. Companion model BS-06, Billerica, MA, USA). Solids were dissolved in 200 μL of acetonitrile (Hiai et al., 1976). For total saponin quantification, 50 μL of each sample was mixed with 500 μL of vanillin (8 % w/v) and 5 mL of sulphuric acid (72 % v/v). Samples were incubated at 60 °C for 10 min and cooled in an ice water bath. Absorbance was read at 538 nm, and results were expressed as micrograms of oleanolic acid equivalents per microgram (μg OAE/g), using a calibration curve of 0–0.109 mg/mL (R^2 =0.99).

2.6.5. Total carotenoids

For the total carotenoids extraction, 5 mg of the sample was mixed with acetonitrile:methanol:tetrahydrofuran solution (50:45:5 v/v/v), and was shaken for 2 h. Samples were centrifuged at 8000 g for 5 min at 5 °C. The absorbance of the supernatants was read at 450 nm (Jorge et al., 2014). Results were expressed in mg equivalents of β-carotene per gram of dry sample (mg βCE/g).

2.6.6. Antioxidant capacity by DPPH and ABTS free radical scavenging

The antioxidant capacity assessment was evaluated by the ability of samples to scavenge the stable radical 1,1-diphenil-2-picrylhydrazyl (DPPH) according to Xu and Chang (2007). Briefly, 100 μL of the acetonic extract previously described was mixed with 1 mL of DPPH ethanol solution 0.1 mM. The mixture was left at room temperature in the dark, thereafter the absorbance was measured at 517 nm against an ethanol blank. Additionally, the 2.2-azinobis (3-ethyl-benzothiazoline-6-sulphonic) diammonium salt (ABTS) free radical scavenging capacity of samples was evaluated following Managa et al. (2020). The ABTS radical solution was prepared by adding ABTS to 0.1 mM phosphate buffer pH=7.4 and potassium persulfate 2.45 mM. Afterward, the mixture was held in darkness for 16 h at 25 °C and diluted with 0.1 the phosphate buffer until an absorbance of 0.70 ± 0.03 was obtained at 734 nm; then, 100 μL of the acetonic extract was mixed with 1 mL of the radical solution. The absorbance of samples and a control (100 phosphate buffer instead of sample) was read at 734 nm. Results were expressed as mg equivalent of trolox per gram (mg ETX/g) for both assays.

2.6.7. Inhibition of digestive enzymes

2.6.7.1. α-amylase. The α-amylase inhibition capacity was evaluated according to Kandra et al. (2005). Briefly, 50 μL of the acetonic extract was incubated with 50 μL of α-amylase from *Bacillus subtilis* (50 units/mg) in a water bath at 37 °C for 20 min. Afterwards, 100 μL of a

1 % starch solution prepared in phosphate buffer at pH 7.0 with 38 mM NaCl were added, and the whole mixture was incubated for 2 h. Total glucose was quantified using a GOD-PAP kit following kit instructions.

2.6.7.2. Pancreatic lipase. Porcine pancreatic lipase type II was dissolved in distilled water (10 mg/mL). The supernatant was recovered after the solution centrifugation at 13,000 rpm for 5 min. The buffer used for the determination was 100 mM Tris buffer (pH 8.2) and p-nitrophenyl laurate (PNP) as a substrate at a concentration of 0.08 % dissolved in 5 mM sodium acetate (pH 5.0) with 1 % Triton X-100. The solution was heated for 1 min in boiling water, and then, mixed well and cooled at room temperature. For the determination, each tube contained 400 μL of the assay buffer, 450 μL of the substrate solution, and 150 μL of pancreatic lipase and we added 450 μL of the prickly-pear-peel extracts. The samples were incubated at 37 °C for 2 h, then centrifuged at 13,000 rpm for 2.5 min and the absorbance was read at 400 nm in a MultiScan Go, according to McDougall et al.(2009). Both α-amylase and pancreatic lipase inhibition capacities were calculated.

2.7. Statistical analysis

Phytochemical data were analyzed in a complete randomized model using the general linear model procedure of the statistical analysis system (SAS Institute ver. 9.4, 2002–2010, Cary, NC, USA). Treatment means were grouped by the least significant difference of Fisher's test at $p \leq 0.05$.

3. Results and discussion

3.1. Thermal characterization of IR dryer

Table 2 shows some of the thermal variables recorded during the operation of the IR dryer. During the drying experiments, the laboratory air temperature (T_{room}) and relative humidity (RH_{room}) ranged from 17 to 21 °C and from 25 to 55 %, respectively. The incident IR energy, as well as the temperature of the emitter, the air, and the maximum temperature of the sample, showed a directly proportional relationship with the supply pressure of the emitter (Experiment I) and an inversely proportional relationship with the distance between the emitter and the sample (Experiment II). The temperature of the hot air generated by the emitter varied in a range of 58 to 80 °C with a velocity between 0.88 and 2.77 m/s. The maximum temperature reached by the cactus samples was between 60 and 89 °C. The maximum internal temperatures reached in the cactus samples exceeded the temperatures of the hot air flow generated by the emitter. This result indicates a possible synergistic effect resulting from the use of CIR emitters compared to the conventional HA technique. Such synergy could be attributed to the efficient direct energy transfer inherent to IR technology, which favors a more pronounced thermal increase in the plant material and, consequently, an acceleration of the dehydration process. These results emphasize the influence of operating conditions on the thermal characteristics of the drying process, providing a quantitative basis for the association between the incident IR energy and the thermal response observed in the cactus samples.

In the experiments I (Fig. 3A) and II (Fig. 3B), the internal temperature of the cladode samples was intrinsically linked to the relative water content (RWC), that is, to the proportion of water in the sample concerning the initial content, which observed three phases. The first phase was recorded at the beginning of the drying process, where a rapid increase in the internal temperature of the samples between 30 and 38 °C was observed, with <20 % of the water evaporating. The second phase experienced a sustained gradual increase in the temperature of the cactus samples, during which 80 % of the water evaporated. The final phase involves the elimination of the last 20 % of humidity and was characterized by an accelerated rise in temperature. This phenomenon is explained by the water retention capacity in the plant tissues, as at the end of the drying process, the water molecules are retained at a low (more negative) water potential in the plant tissues, and therefore, a higher temperature is required to remove the water molecules retained in the tissue (Guo et al., 2022). This behavior supports the findings of (Nowak & Lewicki, 2004), who observed similar results during the drying of apple slices with IR energy. The proper combination of gas supply pressure and distance between emitter and sample helps establish the temperature for optimal drying of vegetative material. In this case, gas supplementation at 50 mbar at a distance of 38.0 cm (level III) resulted in a final plant tissue temperature of 60.53 °C, which could be compared with the drying process of plant tissue with HA at 65 °C (Medina-Torres et al., 2008). HA-IR drying at high incident energy can be particularly effective during the first phases of the process, while at the end of the process, it must be decreased to ensure not exceeding the permissible temperature that guarantees product quality.

3.2. Drying kinetics and drying time

The average moisture content of fresh slice samples of cactus cladodes was 91.64 ± 1.41 % (wet basis). Meanwhile, the dry samples reached a final average moisture content of 10.56 ± 0.52 % across the different tests. The variations in moisture content as a function of drying time for the two experimental configurations are shown in Fig. 4. It was observed that both the supply pressure (IR energy intensity) and the distance between the emitter and the product were important variables affecting the drying time of the cladode slices. Investigating the drying time is important because it influences the quality of the product, energy consumption, and, consequently, production costs. For both experimental configurations, the moisture content gradually decreased as a function of drying time, but starting at 80 % moisture content, the water removal was greater until it stabilized when the samples reached 10 % moisture content. It has been reported that the drying time decreases with increasing IR intensity in drying slices of eggplant (Jafari et al., 2020), apple (EL-Mesery et al., 2021), and garlic (EL-Mesery et al.,

Table 2
Operating conditions during IR drying experiments.

Experiment/treatments	T_{room} (°C)	RH_{room} (%)	Incident IR energy (W/m^2)*	Temperatures (°C)		
				Emitter	Air	$Samples_{max}$
Experiment I						
70 mbar	17.7	46.2	2432.6 ± 3.4	140.6	64.5	76.5
80 mbar	20.4	35.2	2615.5 ± 9.7	153.1	71.3	82.5
90 mbar	21.4	33.6	2794.6 ± 5.4	160.1	74.8	84.1
100 mbar	19.9	42.8	2960.1 ± 5.6	169.3	76.5	85.5
110 mbar	16.9	55.6	3096.4 ± 6.8	175.4	80.5	89.8
Experiment II/Level						
14.0 (I)	19.8	27.1	4304.7 ± 10.7	135.7	60.5	82.1
24.0 (II)	17.1	25.4	3124.7 ± 3.8	133.3	58.8	72.9
38.0 (III)	18.8	45.6	2185.9 ± 4.7	134.3	59.5	60.5

* Incident IR energy values are expressed as mean ± standard deviation.

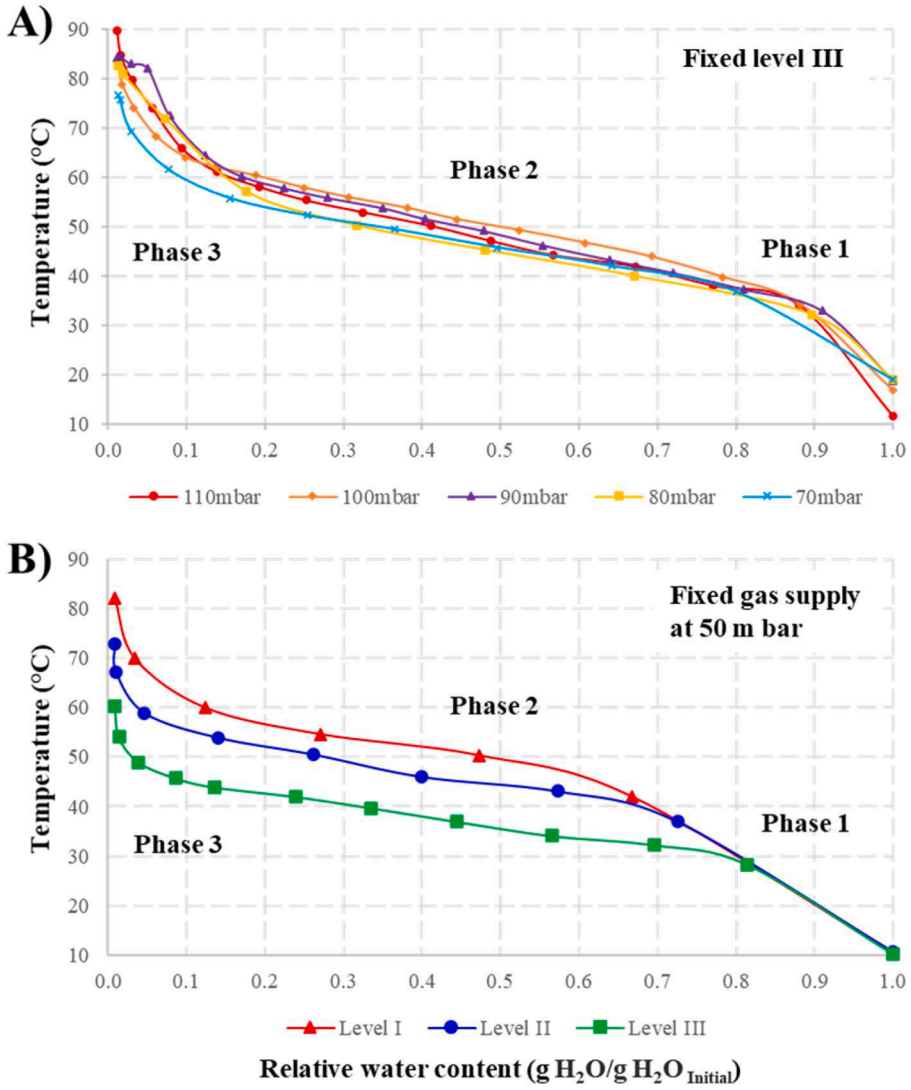

Fig. 3. Changes in relative water content and cladode slices internal temperature during the experiments I A) and II B).

2022). Meanwhile, increasing the distance between the emitter and the product increased the drying time of apple slices (Nowak & Lewicki, 2004) and mint leaves (Salarikia et al., 2017). The behavior observed in the tests varying the distance was consistent with previous studies, as shown in Fig. 4B, where an increase of 1.7 times the distance of level I resulted in an 83 % increase in drying time. However, for the tests varying the supply pressure (IR intensity), the behavior was not as expected. Fig. 4A, shows that the fastest loss of moisture content occurred at a supply pressure of 80 mbar with a drying time of 70 min (2615.51 ± 9.65 W/m^2). Meanwhile, the drying times for the tests with 90, 100, and 110 mbar, with higher incident energy, were longer (85, 80, and 75 min, respectively). This adverse effect can be attributed to very rapid drying on the surface of the samples, which generates a hard crust that increases water transport resistance from the sample's interior (Maskan, 2001), thereby increasing the drying time. Avoiding the crusting phenomenon prevents the increase in hardness (Liu et al., 2021). This leads to the almost total elimination of water retained inside the slice samples of the cladodes. This minimizes the accumulation of non-volatile compounds that eventually would induce oxidation or browning in the samples (Tello-Ireland et al., 2011), which would detract from the cladode powder quality. Wu et al. (2023) have reported crust formation on the carrot slices' surface during CIR emitter processing. Therefore, our findings indicate that to avoid the formation of a sealing surface that prevents drying inside the cladode slice samples, it is necessary to gradually dry using lower IR intensities of 2615 W/m^2 at the beginning of the process.

The drying rate as a function of drying time and moisture content in a dry basis is presented for two experimental configurations: i) varying the gas supply pressure (Experiment I), shown in Fig. 5A and 5C; and ii) varying the distance between the catalytic emitter and the samples (Experiment II), illustrated in Fig. 5B and 5D For the configuration varying the supply pressure, the highest drying rate was 0.26 g water/g dry matter per min when exposed to the 100-mbar treatment (Fig. 5A). For the configuration varying the distance, the highest drying rate was 0.44 g water/g dry matter per min with the Level I treatment (Fig. 5B). It can be seen that, for most of the treatments, a constant drying period was not exhibited under the experimental conditions; instead, they showed a decreasing drying period, except for the Level III and 50 mbar treatment that maintained a constant drying rate between 20 and 70 min. This exception could be due to lower heat flux, resulting in a longer time to reach the critical moisture content. The absence of a constant rate period is in agreement with observations in IR drying of blueberries (Shi et al., 2008), apples (EL-Mesery et al., 2021), and garlic (EL-Mesery et al., 2022). Furthermore, this behavior is similar to hot air drying of prickly pear peels (Lahsasni et al., 2004). This phenomenon is often attributed to a different water supply from the product surface (EL-Mesery et al., 2022) and because the thin product layer does not provide a constant water supply (Shi et al., 2008). Additionally, surface drying can occur

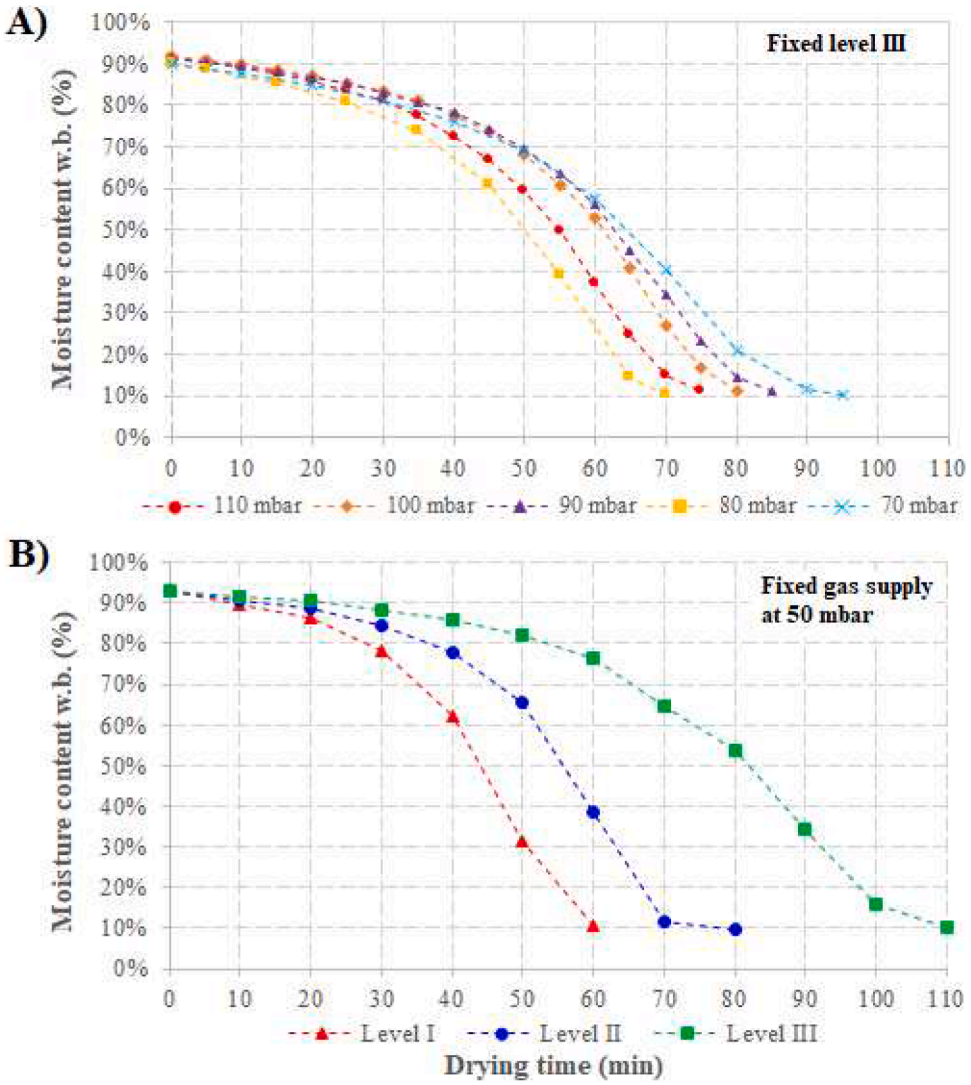

Fig. 4. Drying curves of slices of cactus cladodes in Experiments I A) and II B).

more rapidly with CIR drying, resulting in a faster entry into the rate of decline period due to the slow diffusion of water to the product surface (Gabel et al., 2006). The trend of decreasing drying rate over time can be explained because moisture was drawn from larger capillaries in the first stage of the decay period, followed by smaller capillaries, which led to a decrease in the evaporation rate. IR radiation is a type of non-contact heat transfer, in which energy is directly absorbed by the molecules of the material to be dried. Consequently, drying times are shorter compared to hot air (HA) drying. For instance, Medina-Torres et al. (2008) reported drying times between 660 and 972 min for 5 mm cactus pear cladodes slices in a laboratory HA dryer, while García-Valladares et al. (2020) reported a drying time of 360 min using a semi-industrial indirect solar dryer. In contrast, previous studies on HA-IR drying of apples have reported drying times ranging from 135 to 250 min, depending on drying conditions (El-Mesery et al., 2023; EL-Mesery et al., 2021; El-Mesery & Mwithiga, 2015). Similarly, Feng et al. (2019) documented drying times of 150–240 min for 3 mm garlic slices using a catalytic infrared radiation (CIR) dryer. Regarding cactus pear cladodes, Touil et al. (2010) reported a drying time of 275 min for 10 mm cubes using an IR-electric dryer, with a maximum drying rate of 0.0135 g/g-min. In the present study, drying times ranged from 60 to 110 min under different CIR drying conditions (Level I-50 mbar and Level III-50 mbar treatments, respectively). These results highlight the potential of CIR drying to significantly reduce drying time compared to other technologies, particularly for cactus pear cladodes.

3.3. *Drying curves fitting*

Alternatively, to the lack of fit test, Neter et al. (1983) point out that the highest values of R^2, the lowest RMSE values, and the significance (χ^2) of the coefficients included in a fitting curve can be used as indicators of the model's performance. This was the criterion used to select the best model to estimate and represent the rate of moisture loss during the dehydration of cladode slices by HA-IR in the range of observed data. The empirical constants generated for each model and the statistics associated with each evaluated model are indicated in Tables 3 and 4, respectively. In all cases, the R^2 values for the tested models were higher than the threshold established by Erenturk et al. (2004) ($R^2 = 0.90$), along with significant χ^2 and RMSE values, which were indicative of a good fit (Table 4).

The Page, Logarithmic, and Midilli-Kucuk models stood out in terms of predictive capacity due to their high R^2 and low χ^2 and RMSE values. This was particularly evident with the Midilli-Kucuk model, which provided the best fit for the drying kinetics of the studied plant material (Table 4). In other studies, this model was also found suitable for describing the drying behavior of prickly pear peels using forced convection with hot air (Lahsasni et al., 2004) and for drying nopal cladode cubes using IR-electric dryers (Touil et al., 2010). Unlike the Page

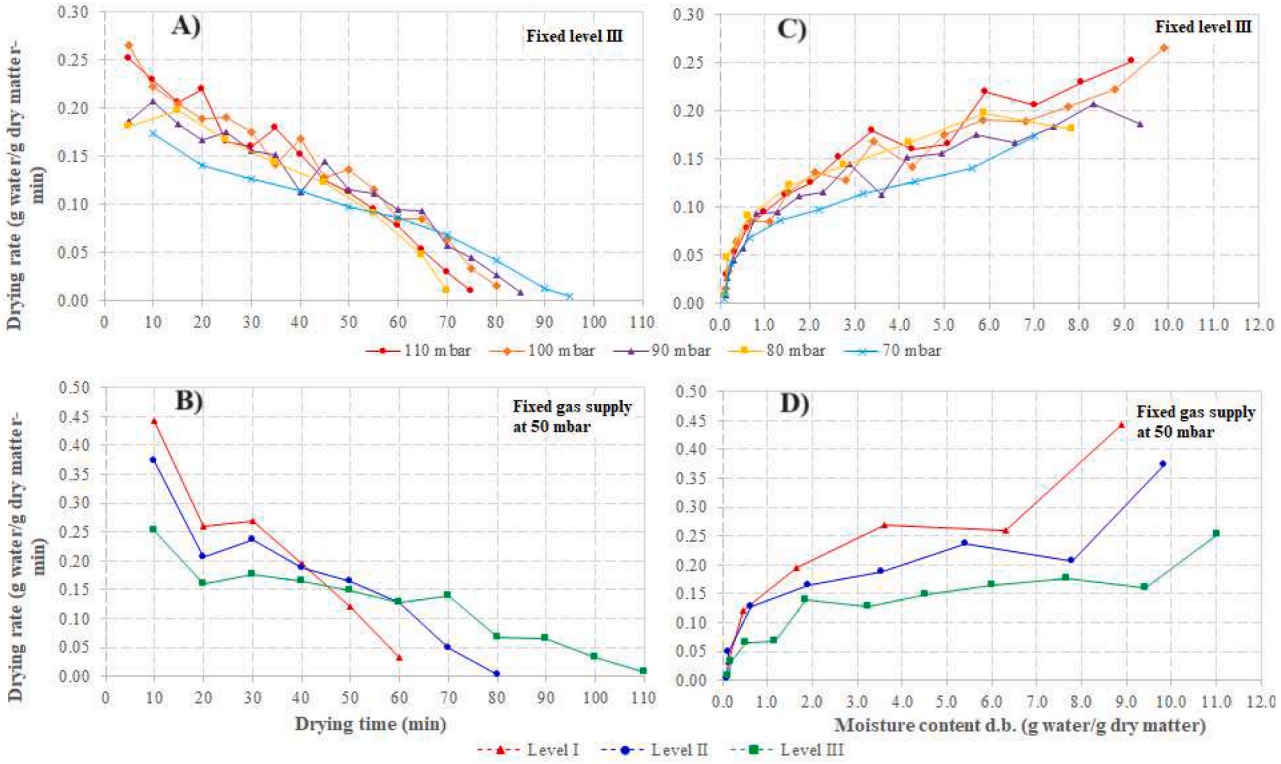

Fig. 5. Changes in the drying rate of cactus pear cladode slices over time by varying gas supply pressure (Experiment I, A) and the distance between the catalytic emitter and the drying samples (Experiment II, B). Changes in the drying rate of cactus pear cladode slices by moisture content, varying gas supply pressure (Experiment I, C) and the distance between the catalytic emitter and the drying samples (Experiment II, D).

Table 3
Constants and regression coefficients (ϕ) of thin-layer drying models.

Models	ϕ	Experiment I					Experiment II		
		70 mbar	80 mbar	90 mbar	100 mbar	110 mbar	Level I	Level II	Level III
Newton	*k*	0.0279	0.0355	0.0287	0.0305	0.0337	0.0452	0.0352	0.0238
Page	*k*	0.0077	0.0077	0.0068	0.0095	0.0101	0.0180	0.0121	0.0058
	n	1.3430	1.4321	1.3900	1.3241	1.3430	1.2788	1.2977	1.3611
Henderson and Pabis	*k*	0.0293	0.0375	0.0310	0.0324	0.0358	0.0463	0.0364	0.0250
	a	1.0537	1.0605	1.0805	1.0609	1.0652	1.0273	1.0373	1.0559
Logarithmic	*k*	0.0188	0.0232	0.0174	0.0174	0.0202	0.0313	0.0265	0.0151
	a	1.2375	1.2694	1.3557	1.3835	1.3495	1.1989	1.1504	1.2851
	c	−0.2248	−0.2466	−0.3342	−0.3794	−0.3381	−0.1982	−0.1423	−0.2759
Midilli y Kucuk	*k*	0.0110	0.0103	0.0099	0.0153	0.0149	0.0279	0.0149	0.0082
	a	0.9912	0.9916	0.9897	0.9910	0.9913	0.9961	0.9861	0.9835
	b	−0.0008	−0.0008	−0.0012	−0.0019	−0.0016	−0.0016	−0.0006	−0.0008

model, the Logarithmic and Midilli-Kucuk models generated negative MR values towards the final stages of drying for most of the studied conditions, which is physically impossible. The last is indicative that these models are underestimating the observed values due to overfitting and misleadingly high R^2 values (Neter et al., 1983).

3.4. Phytochemical attributes and functionality assessments of cactus pear cladode slices

3.4.1. Phytochemical analysis experiment I

The LP gas supply pressures at either 80 or 90 mbar produced the highest insoluble dietary fiber and resistant starch, and total dietary fiber and soluble dietary fiber, respectively (Table 5). As mentioned before, thermal treatment is likely to produce structural changes in this type of compound, however, the current results show that the concentration of non-digestible carbohydrates is dependent on the pressure of the LP gas supply. Pressure processing can alter the noncovalent bonds of the dietary fiber in foods, and its soluble and insoluble fractions, thereby inducing changes in their structural characteristics, therefore, the molecules bound to the fiber matrix such as polyphenols (Zhao et al., 2024). Nonetheless, the LP gas supply pressure did not affect the content of total phenols, flavonoids, and condensed tannins (Table 5).

Regarding the total saponins content, according to Yang et al. (2022), high-temperature and high-pressure thermal processing increased the bioactive components of ginsenosides (also known as steroid-like saponins) evaluated in *Panax ginseng*. The highest concentration of saponins was observed among the 70 and 90 mbar, with no-statistical difference ($p < 0.05$). Hence, following up the effect of gas supply pressures, an intermediate pressure (80–90 mbar) led to high accumulation of several phytochemicals, not including total carotenoids. In this regard, a high pressure in the LP gas supply represents a more heated drying environment, which may influence the humidity of samples. Higher relative humidity may eventually lower the internal temperature of the sample and lead to increased retention of

Table 4
Statistical parameters were determined from the fitting of several thin-layer empirical equations. Coefficient of determination (R^2), chi-square (χ^2), and root mean square error (RMSE).

Models	Parameters	Fixed gas supply at 50 mbar					Fixed Level III		
		70 mbar	80 mbar	90 mbar	100 mbar	110 mbar	Level I	Level II	Level III
Newton	R^2	0.9668	0.9635	0.9523	0.9622	0.9615	0.9774	0.9716	0.9598
	χ^2	3.10E-03	4.04E-03	3.73E-03	2.95E-03	3.10E-03	2.59E-03	2.87E-03	3.59E-03
	RMSE	0.0531	0.0603	0.0594	0.0526	0.0538	0.0471	0.0508	0.0574
Page	R^2	0.9948	0.9965	0.9945	0.9934	0.9946	0.9929	0.9912	0.9924
	χ^2	6.80E-04	5.56E-04	6.14E-04	7.15E-04	6.04E-04	1.12E-03	1.19E-03	9.60E-04
	RMSE	0.0236	0.0211	0.0234	0.0258	0.0229	0.0283	0.0308	0.0283
Henderson and Pabis	R^2	0.9748	0.9736	0.9694	0.9732	0.9735	0.9800	0.9757	0.9692
	χ^2	2.96E-03	3.77E-03	3.05E-03	2.59E-03	2.67E-03	2.93E-03	2.99E-03	3.43E-03
	RMSE	0.0492	0.0549	0.0520	0.0492	0.0481	0.0457	0.0489	0.0535
Logarithmic	R^2	0.9970	0.9963	0.9976	0.9991	0.9986	0.9971	0.9929	0.9958
	χ^2	4.49E-04	6.70E-04	2.88E-04	1.02E-04	1.75E-04	5.78E-04	1.10E-03	5.87E-04
	RMSE	0.0181	0.0217	0.0155	0.0094	0.0118	0.0182	0.0278	0.0210
Midilli y Kucuk	R^2	0.9981	0.9988	0.9989	0.9993	0.9991	0.9971	0.9943	0.9970
	χ^2	3.12E-04	2.56E-04	1.45E-04	9.24E-05	1.13E-04	7.84E-04	1.04E-03	4.78E-04
	RMSE	0.0141	0.0124	0.0106	0.0086	0.0091	0.0183	0.0250	0.0178

Table 5
Influence of LP gas supply pressures (GSPs) on phytochemicals content. The corresponding incident infrared energy (IIR, W/m^2) values per each temperature is given. Phenolic compounds: total phenols (TP), flavonoids (FV), and condensed tannins (CT).

	GSPs (mbar)/IIR (W/m^2)					LSD	Significance	CV (%)
	70/(2428.9)	80/(2603.5)	90/(2775.7)	100/(2916.4)	110/(3059.0)		($P > F$)	
Non-digestible carbohydrates (g/100 g)								
Total dietary fiber	14.0 ± 0.7c	15.9 ± 0.2b	21.3 ± 0.6a	11.1 ± 0.1d	9.4 ± 0.03e	1.489	< 0.0001	4.0
Soluble dietary fiber	7.2 ± 0.9a	1.3 ± 0.3b	7.7 ± 0.7 a	0.7 ± 0.02b	1.4 ± 0.2b	1.85	0.0004	19.7
Insoluble dietary fiber	6.9 ± 0.2e	14.6 ± 0.2a	13.6 ± 0.1b	10.4 ± 0.1 c	8.0 ± 0.2d	0.6	< 0.0001	2.2
Resistant starch	4.2 ± 0.1e	8.9 ± 0.1a	8.1 ± 0.01b	6.5 ± 0.03c	4.7 ± 0.2d	0.338	< 0.0001	2.0
Phenolic compounds								
TP (mg GAE/g)	0.2 ± 0.005 a	0.2 ± 0.013 a	0.2 ± 0.009 a	0.2 ± 0.005 a	0.2 ± 0.016 a	0.037	0.275	6.6
FV (mg CAE/g)	0.4 ± 0.019 a	0.5 ± 0.047 a	0.5 ± 0.014 a	0.5 ± 0.0 a	0.5 ± 0.005a	0.085	0.566	7.3
CT (mg CAE/g)	4.6 ± 0.8 a	5.1 ± 0.2 a	4.1 ± 0.02 a	4.3 ± 0.1 a	4.5 ± 0.0 a	1.3184	0.4364	11.3
Saponins (μg OAE/g)	4.6 ± 0.1 a	4.3 ± 0.0 a	4.7 ± 0.2 a	3.8 ± 0.1 b	3.8 ± 0.02 b	0.403	0.0074	3.7
Carotenoids (mg βCE/g)	54.8 ± 0.2 a	44.6 ± 2.1 c	47.1 ± 0.4 c	51.1 ± 0.6 b	46.9 ± 0.2 c	3.645	0.0045	2.9

Values are expressed as mean ± standard deviation. Different letters within columns indicate significant difference by the least significant difference (LSD) of Fisher's test at $p < 0.05$.

carotenoids, as higher relative humidity leads to slower β-carotene decomposition or alterations in their molecular structure; thus, a decrease in their chemical reactivity or/and an increase in their extractability in their analysis due to deceased polymerization (Sarpong et al., 2019). Interestingly, although the lowest pressure supply (70 mbar) leads to the highest carotenoid concentration, 100 mbar dried cladode slices exhibit higher concentration than 80 and 90 mbar LP supply. Because carotenoids are thermolabile, to avoid the loss of pigments belonging to this group by traditional thermal treatments, High-pressure high-temperature (HPHT) processing is being developed. However, the pressure and temperature application leads to a softening of the plant tissue and denaturation of protein complexes located in the chloroplasts that could help to release carotenoids from the vegetable matric (Sánchez et al., 2014).

3.4.2. Functional properties experiment I

The LP gas supply pressures at either 100 or 110 mbar produced the highest antioxidant capacity, in terms of ABTS and DPPH scavenging (Table 6). In contrast, the lowest LP gas supply pressure produced the greater inhibition of digestive enzymes, like α-amylase and pancreatic lipase (Table 6).

3.4.3. Phytochemical analysis experiment II

The highest non-digestible carbohydrate contents were found at a distance of 24.0 cm (distance II) between the emitter and the cladode sample (Table 7). However, at a greater distance (38.0 cm), no significant ($p > 0.05$) differences were found for the concentration of insoluble dietary fiber and resistant starch. Consuming fiber- and resistant starch-rich foods contributes to regulating some chronic diseases such as obesity, and decreases blood glucose, triglycerides, and LDL due to the production of short-chain fatty acids by colonic fermentation (Herrera, Reynoso-Camacho et al., 2021). Hence, the

Table 6
Influence of LP gas supply pressures (GSPs) on the antioxidant capacity (mg ETX/g) and inhibition of digestive enzymes (%) [α-amylase (α-AM) and pancreatic lipase (PL)].

GSPs (mbar)/IIR (W/m^2)	Antioxidant capacity		Inhibition of digestive enzymes	
	ABTS	DPPH	α-AM	LP
70/(2428.9)	1.3 ± 0.2 b	7.0 ± 0.4 b	20.1 ± 0.2 a	70.5 ± 0.0 a
80/(2603.5)	0.9 ± 0.01 bc	3.2 ± 0.3 c	19.7 ± 0.3 a	64.2 ± 0.03 c
90/(2775.7)	0.1 ± 0.1 c	1.2 ± 0.7 d	20.4 ± 0.2 a	54.9 ± 0.1 d
100/(2916.4)	3.8 ± 0.6 a	7.9 ± 0.0 ab	16.3 ± 0.1 b	68.5 ± 0.2 b
110/(3059.0)	3.9 ± 0.7 a	8.6 ± 0.5 a	14.3 ± 0.2 c	68.2 ± 0.0 b
LSD	1.035	1.1685	0.726	0.346
Significance ($P > F$)	0.001	< 0.0001	< 0.0001	< 0.0001
CV (%)	82.23	54.44	1.6	0.2

Values are expressed as mean ± standard deviation. Different letters within columns indicate significant difference by the least significant difference (LSD) of Fisher's test at $p < 0.05$.

Table 7
Influence of the experimental setup at different distances between the emitter and cladode samples on phytochemicals content. Phenolic compounds: total phenols (TP), flavonoids (FV), and condensed tannins (CT).

Compounds	Distance (Level)			LSD	Significance	CV (%)
	14.0 cm (I)	24.0 cm (II)	38.0 cm (III)		($P > F$)	
Non-digestible carbohydrates (g/100 g)						
Total dietary fiber	9.0 ± 0.2b	14.5 ± 0.5a	10.5 ± 0.5b	1.8973	0.0057	5.3
Soluble dietary fiber	2.7 ± 0.2b	5.7 ± 0.5a	1.8 ± 0.04b	1.5036	0.0081	13.9
Insoluble dietary fiber	6.3 ± 0.01b	8.8 ± 0.04a	8.7 ± 0.46a	1.1871	0.0107	4.7
Resistant starch	3.8 ± 0.01b	5.2 ± 0.05a	3.8 ± 0.08a	0.6606	0.0088	4.4
Phenolic compounds						
TF (mg GAE/g)	0.2 ± 0.01 a	0.2 ± 0.02 a	0.2 ± 0.01 a	0.0431	0.118	7.1
FV (mg CAE/g)	0.5 ± 0.04a	0.4 ± 0.04 a	0.4 ± 0.01a	0.1387	0.745	9.8
CT (mg CAE/g)	4.2 ± 0.0 b	5.7 ± 0.2 a	5.2 ± 0.4 ab	1.1171	0.048	7
Saponins (μg OAE/g)	3.8 ± 0.2 b	5.0 ± 0.1 a	3.8 ± 0.1b	0.5883	0.012	4.4
Carotenoids (mg βCE/g)	44.2 ± 0.0 c	67.6 ± 0.3b	71.8 ± 0.4 a	3.4388	0.0002	1.8

Values are expressed as mean ± standard deviation. Different letters within columns indicate significant differences by the least significant difference (LSD) of Fisher's test at $p < 0.05$.

importance of finding food processing technologies that improve its content. It is well known that thermal treatment changes the dietary fiber at a structural level, modifying the insoluble:soluble ratio of the dietary fiber (Ullah et al., 2017). In the case of resistant starch, the mild heat led to more structural stability due to the rearrangement of amylose chains, facilitating the interaction of amylose and amylopectin, thus, conferring a more stable granule, resulting in the increase of resistant starch (Dupuis et al., 2014).

At both the constant angle of the tray inclination (45°) and gas supply pressure (50 mm bar), the content of total phenols and flavonoids were not altered by the distance between the emitter and the cladode sample. In contrast, condensed tannins concentration was augmented as the distance between the emitter and cladode sample increased (Table 7). In the dehydration of *Rubus idaeus* by infrared radiation and microwave vacuum combined-drying technology, Si et al. (2016) mentioned that the changes on some polyphenols can be mainly attributed to the effect of heating and the activity of some enzymes, like the polyphenol oxidase. This enzyme can degrade phenolic compounds; however, mild heating may inactivate it. Interestingly, different cultivars require different processing conditions, for instance, *Saccharum officinarum* and *Fragaria* × *ananassa* require low temperatures (60 °C) to inactivate it (Zawawi et al., 2022). Although disruption of cell walls may trigger the release of the oxidative and hydrolytic enzymes, for some types of phenolics, like condensed tannins, a higher processing temperature may be beneficial to prevent their loss.

The greater saponin content was observed at the intermediate distance (II) between the emitter and cladode sample (Table 7). Little is known about the effects of cooking methods on changes in saponin concentration (Tan et al., 2014). Liu et al. (2020) reported that thermal treatment would modify the total saponin content in *Momordica charantia* L. Moreover, the current results indicate that the distance between the sample and the emitter, thus the direct contact with heat, significantly interferes with the final concentration of these compounds. Meanwhile, the concentrations of carotenoids increased, as so did the distance between the emitter and the cladode sample. In this work, total carotenoids were reported as mg equivalents of β-carotene. Azeez et al. (2019) mentioned that β-carotene decreases significantly with drying temperatures, which is in agreement with the current results; likewise, Demiray et al. (2013) mentioned that drying *Lycopersicon esculentum* resulted in the degradation of β-carotene, as degradation rate increased with temperature augmentations.

3.4.4. Functional properties experiment II

Concerning the functional properties of the dried cladode samples, the greatest distance (III) between the emitter and cladode sample had the greater antioxidant capacity, by ABTS scavenging; but the shorter distance (I) had the greater capacity to scavenge the DPPH free radical. The opposite occurred with the digestive enzyme inhibition, in terms of α-amylase and pancreatic lipase, respectively (Table 8). Antioxidant activity variations among treatments could be attributed to the degradation caused by enzyme and heating, which led to the loss of antioxidants with a greater capacity to scavenge the DPPH radical. However, intermediate products by degradation and Maillard reaction can improve antioxidant ability, which may be the case for the observation of ABTS scavenging capacity (Si et al., 2016). To the best of our knowledge, there is a lack of information of how thermal processing may affect the capacity of foods to inhibit digestive enzymes. The fundament might be similar to that of the antioxidant capacity, the higher the distance between the emitter and the cladodes (38.0 cm), the higher the capacity to inhibit the lipase activity, and this might be related to the higher concentration of some non-digestible carbohydrates and carotenoids of samples dried under this condition. The inhibition of digestible enzymes is a desirable result when evaluating the functional potential of foodstuff, since evaluating the inhibition capacity of *in vitro* digestive enzymes like α-amylase and pancreatic lipase is a preliminary approach to determine its functional potential. The α-amylase hydrolyzes oligosaccharides to glucose, while pancreatic lipase hydrolyzes triglycerides to free fatty acids, therefore, the digestive enzymes inhibition could reduce glucose and lipid absorption (Herrera, Zegbe et al., 2021).

4. Conclusions

The influence of operating conditions on the drying of cactus pear cladode slices using a catalytic infrared (CIR) dryer was investigated. By controlling the LP gas supply pressure and the distance between the emitter and the samples, the intensity of the infrared energy could be adjusted, which impacted the drying process and the bioactive

Table 8
Influence of the experimental setup at different distances between the emitter and cladode samples on the antioxidant capacity (mg ETX/g) and inhibition of digestive enzymes (%) [α-amylase (α-AM) and pancreatic lipase (PL)].

	Antioxidant capacity		Inhibition of digestive enzymes	
Distance (Level)	ABTS	DPPH	α-AM	LP
14.0 cm (I)	1.59 ± 0.03 b	5.1 ± 0.2 a	11.6 ± 0.02 a	70.5 ± 0.1 c
24.0 cm (II)	1.93 ± 0.4 b	3.4 ± 0.2 b	8.0 ± 0.6 b	72.6 ± 0.3 b
38.0 cm (III)	4.0 ± 0.4 a	3.9 ± 0.4 b	7.5 ± 0.1b	73.8 ± 0.2 a
LSD	0.9427	0.7965	1.5824	1.0168
Significance ($P > F$)	0.007	0.0133	0.0069	0.0045
CV (%)	47.50	19.71	5.5	0.4

Values are expressed as mean ± standard deviation. Different letters within a column indicate significant differences by the least significant difference (LSD) of Fisher's test at $p < 0.05$.

compounds concentration of the cladode slices. The empirical Page's model (R^2 = 0.99) best described the drying process. Additionally, variations in gas pressure and emitter distance positively influenced non-digestible carbohydrates, phenolic compounds, antioxidant capacity, and inhibition of digestive enzymes. Overall, our initial hypothesis is in agreement with the obtained results, using an LP gas catalytic emitter, will maintain or improve the quality of the dried product by retaining bioactive compounds and preserving its the functional properties, while reducing drying time compared to the conventional hot air-drying methods. This study highlights the potential of emerging drying technologies for agricultural products, contributing to food security and human health.

Ethical statement

No studies with animals or humans were conducted.

Funding

This research was funded, in part, by the Consejo Nacional de Humanidades, Ciencias y Tecnologías (CONAHCYT) PRONACES-FOP04–2021–03 project No 319,195, and by the Instituto Nacional de Investigaciones Forestales, Agrícolas y Pecuarias (INIFAP) grant No SIGI: 8403,134,459 to Dr. Jorge A. Zegbe.

CRediT authorship contribution statement

Néstor Manuel Ortiz-Rodríguez: Writing – original draft, Validation, Resources, Methodology, Investigation, Data curation, Conceptualization. **Mayra Denise Herrera:** Writing – review & editing, Writing – original draft, Validation, Resources, Methodology, Investigation, Data curation, Conceptualization. **Jorge A. Zegbe:** Writing – review & editing, Writing – original draft, Validation, Resources, Project administration, Methodology, Investigation, Funding acquisition, Data curation, Conceptualization. **Luis Roberto Reveles-Torres:** Writing – review & editing, Resources, Project administration, Funding acquisition. **Nicolás Iván Román-Roldán:** Visualization, Supervision, Resources, Investigation, Conceptualization.

Declaration of competing interest

The authors declare that they have no known competing financial interests or personal relationships that could have appeared to influence the work reported in this paper.

Acknowledgements

We thank MBA Juan José Urbano-Castelán and Dr David Riveros-Rosas of Solar and Thermal Solutions, S.A. de C.V., Co. for the instrumentation facilities.

Supplementary materials

Supplementary material associated with this article can be found, in the online version, at doi:10.1016/j.afres.2025.100867.

Data availability

Data will be made available on request.

References

Amaya-Vélez, Y., Roa-Acosta, D. F., Nieto-Calvache, J. E., & Agudelo-Laverde, L. M. (2024). Alternative drying method for chontaduro pulp (*Bactris gasipaes*) by pulsed microwaves: Physicochemical analysis and kinetic model. *Applied Food Research, 4*(2), Article 100556. https://doi.org/10.1016/j.afres.2024.100556. Article.

Ayadi, M., Abdelmaksoud, W., Ennouri, M., & Attia, H. (2009). Cladodes from *Opuntia ficus indica* as a source of dietary fiber: Effect on dough characteristics and cake making. *Industrial Crops and Products, 30*(1), 40–47. https://doi.org/10.1016/j.indcrop.2009.01.003

Azeez, L., Adebisi, S. A., Oyedeji, A. O., Adetoro, R. O., & Tijani, K. O. (2019). Bioactive compounds' contents, drying kinetics and mathematical modelling of tomato slices influenced by drying temperatures and time. *Journal of the Saudi Society of Agricultural Sciences, 18*(2), 120–126. https://doi.org/10.1016/j.jssas.2017.03.002

Bahammou, Y., Tagnamas, Z., Lamharrar, A., & Idlimam, A. (2019). Thin-layer solar drying characteristics of Moroccan horehound leaves (*Marrubium vulgare* L.) under natural and forced convection solar drying. *Solar Energy, 188*, 958–969. https://doi.org/10.1016/j.solener.2019.07.003

Barka, N., Abdennouri, M., El Makhfouk, M., & Qourzal, S. (2013). Biosorption characteristics of cadmium and lead onto eco-friendly dried cactus (*Opuntia ficus indica*) cladodes. *Journal of Environmental Chemical Engineering, 1*(3), 144–149. https://doi.org/10.1016/j.jece.2013.04.008

Bouazizi, S., Montevecchi, G., Antonelli, A., & Hamdi, M. (2020). Effects of prickly pear (*Opuntia ficus-indica* L.) peel flour as an innovative ingredient in biscuits formulation. *Lwt, 124*, Article 109155. https://doi.org/10.1016/j.lwt.2020.109155. Article.

Boukid, F., Boukid, Z., & Mejri, M. (2015). *Opuntia* cladodes: Physicochemical parameters, functional properties and application in formulation of rolled cake of cladode flour fabric (Part 2). *International Journal of Advanced Trends in Computer Science and Engineering, 1*(4), 30–34.

Chen, C., Chaudhary, A., & Mathys, A. (2020). Nutritional and environmental losses embedded in global food waste. *Resources, Conservation and Recycling, 160*, Article 104912. https://doi.org/10.1016/j.resconrec.2020.104912. Article.

Cruz-Rubio, J. M., Mueller, M., Loeppert, R., Viernstein, H., & Praznik, W. (2020). The effect of Cladode drying techniques on the prebiotic potential and molecular characteristics of the mucilage extracted from *Opuntia ficus-indica* and *Opuntia joconostle*. *Scientia Pharmaceutica, 88*(4), 43. https://doi.org/10.3390/scipharm88040043

Das, I., & Das, S. (2010). *Emitters and infrared heating system design*. Boca Raton, FL: CRC Press. https://doi.org/10.1201/9781420090994-c4

de Albuquerque, J. G., de Souza Aquino, J., de Albuquerque, J. G., de Farias, T. G. S., Escalona-Buendía, H. B., Bosquez-Molina, E., & Azoubel, P. M. (2019). Consumer perception and use of nopal (*Opuntia ficus-indica*): A cross-cultural study between Mexico and Brazil. *Food Research International, 124*, 101–108. https://doi.org/10.1016/j.foodres.2018.08.036

Demiray, E., Tulek, Y., & Yilmaz, Y. (2013). Degradation kinetics of lycopene, β-carotene and ascorbic acid in tomatoes during hot air drying. *LWT-Food Science and Technology, 50*(1), 172–176. https://doi.org/10.1016/j.lwt.2012.06.001

Dupuis, J. H., Liu, Q., & Yada, R. Y. (2014). Methodologies for increasing the resistant starch content of food starches: A review. *Comprehensive reviews in food science and food safety, 13*(6), 1219–1234. https://doi.org/10.1111/1541-4337.12104

El-Mesery, H. S., Ashiagbor, K., Hu, Z., & Alshaer, W. (2023). A novel infrared drying technique for processing of apple slices: Drying characteristics and quality attributes. *Case Studies in Thermal Engineering, 52*, Article 103676. https://doi.org/10.1016/j.csite.2023.103676. Article.

EL-Mesery, H. S., Kamel, R. M., & Emara, R. Z. (2021). Influence of infrared intensity and air temperature on energy consumption and physical quality of dried apple using hybrid dryer. *Case Studies in Thermal Engineering, 27*, Article 101365. https://doi.org/10.1016/j.csite.2021.101365. Article.

El-Mesery, H. S., & Mwithiga, G. (2015). Performance of a convective, infrared and combined infrared-convective heated conveyor-belt dryer. *Journal of food science and technology, 52*, 2721–2730. https://doi.org/10.1007/s13197-014-1347-1

EL-Mesery, H. S., Sarpong, F., Xu, W., & Elabd, M. A. (2022). Design of low-energy consumption hybrid dryer: A case study of garlic (*Allium sativum*) drying process. *Case Studies in Thermal Engineering, 33*, Article 101929. https://doi.org/10.1016/j.csite.2022.101929. Article.

El-Safy, F. S. (2013). Evaluation and utilization of cladodes flour in formulating functional sponge cake. *World Applied Sciences Journal, 27*(4), 512–523. https://doi.org/10.5829/idosi.wasj.2013.27.04.81117

Erenturk, S., Gulaboglu, M., & Gultekin, S. (2004). The thin-layer drying characteristics of rosehip. *Biosystems engineering, 89*(2), 159–166. https://doi.org/10.1016/j.biosystemseng.2004.06.002

FAO. (2015). *Pérdidas y desperdicios de alimentos en américa latina y el caribe*. http://www.fao.org/3/a-i4655s.pdf.

Feng, Y., Zhou, C., Yagoub, A. E. A., Sun, Y., Owusu-Ansah, P., Yu, X., Wang, X., Xu, X., Zhang, J., & Ren, Z. (2019). Improvement of the catalytic infrared drying process and quality characteristics of the dried garlic slices by ultrasound-assisted alcohol pretreatment. *Lwt, 116*, Article 108577. https://doi.org/10.1016/j.lwt.2019.108577. Article.

Gabel, M. M., Pan, Z., Amaratunga, K., Harris, L. J., & Thompson, J. F. (2006). Catalytic infrared dehydration of onions. *Journal of Food Science, 71*(9), Article E351-E357. https://doi.org/10.1111/j.1750-3841.2006.00170.x. Article.

García-Valladares, O., Ortiz, N., Pilatowsky, I., & Menchaca, A. (2020). Solar thermal drying plant for agricultural products. *Part 1: Direct air heating system. Renewable Energy, 148*, 1302–1320. https://doi.org/10.1016/j.renene.2019.10.069

Guo, H.-L., Chen, Y., Xu, W., Xu, M.-T., Sun, Y., Wang, X.-C., Wang, X.-Y., Luo, J., Zhang, H., & Xiong, Y.-K. (2022). Assessment of drying kinetics, textural and aroma attributes of Mentha haplocalyx leaves during the hot air thin-layer drying process. *Foods (Basel, Switzerland), 11*(6), 784. https://doi.org/10.3390/foods11060784

Herrera, M. D., Reynoso-Camacho, R., Melero-Meraz, V., Guzmán-Maldonado, S. H., & Acosta-Gallegos, J. A. (2021). Impact of soil moisture on common bean (*Phaseolus vulgaris* L.) phytochemicals. *Journal of Food Composition and Analysis, 99*, Article 103883. https://doi.org/10.1016/j.jfca.2021.103883. Article.

Herrera, M. D., Zegbe, J. A., Melero-Meraz, V., & Cruz-Bravo, R. K. (2021). Functional properties of prickly pear cactus fruit peels undergoing supplemental irrigation and fruit storage conditions. *Plant Foods for Human Nutrition, 76*(4), 427–433. https://doi.org/10.1007/s11130-021-00927-2

Hiai, S., Oura, H., & Nakajima, T. (1976). Color reaction of some sapogenins and saponins with vanillin and sulfur1c acid. *Planta medica, 29*(02), 116–122. https://doi.org/10.1055/s-0028-1097639

Hnin, K. K., Zhang, M., Mujumdar, A. S., & Zhu, Y. (2019). Emerging food drying technologies with energy-saving characteristics: A review. *Drying Technology, 37*(12), 1465–1480. https://doi.org/10.1080/07373937.2018.1510417

Jafari, F., Movagharnejad, K., & Sadeghi, E. (2020). Infrared drying effects on the quality of eggplant slices and process optimization using response surface methodology. *Food chemistry, 333*, Article 127423. https://doi.org/10.1016/j.foodchem.2020.127423. Article.

Jorge, A., Almeida, D. M., Canteri, M. H. G., Sequinel, T., Kubaski, E. T., & Tebcherani, S. M. (2014). Evaluation of the chemical composition and colour in long-life tomatoes (Lycopersicon esculentum Mill) dehydrated by combined drying methods. *International Journal of Food Science & Technology, 49*(9), 2001–2007. https://doi.org/10.1111/ijfs.12501

Kamaraj, S.-K., Rivera, A. E., Murugesan, S., García-Mena, J., Maya, O., Frausto-Reyes, C., Tapia-Ramírez, J., Espino, H. S., & Caballero-Briones, F. (2019). Electricity generation from Nopal biogas effluent using a surface modified clay cup (cantarito) microbial fuel cell. *Heliyon, 5*(4), Article e01506. https://doi.org/10.1016/j.heliyon.2019.e01506. Article.

Kandra, L., Zajácz, Á., Remenyik, J., & Gyémánt, G. (2005). Kinetic investigation of a new inhibitor for human salivary α-amylase. *Biochemical and biophysical research communications, 334*(3), 824–828. https://doi.org/10.1016/j.bbrc.2005.06.165

Krishnamurthy, K., Khurana, H. K., Soojin, J., Irudayaraj, J., & Demirci, A. (2008). Infrared heating in food processing: An overview. *Comprehensive reviews in food science and food safety, 7*(1), 2–13. https://doi.org/10.1111/j.1541-4337.2007.00024.x

Ladha-Sabur, A., Bakalis, S., Fryer, P. J., & Lopez-Quiroga, E. (2019). Mapping energy consumption in food manufacturing. *Trends in food science & technology, 86*, 270–280. https://doi.org/10.1016/j.tifs.2019.02.034

Lahsasni, S., Kouhila, M., Mahrouz, M., Idlimam, A., & Jamali, A. (2004). Thin layer convective solar drying and mathematical modeling of prickly pear peel (Opuntia ficus indica). *Energy, 29*(2), 211–224. https://doi.org/10.1016/j.energy.2003.08.009

Lee, E.-H. (2021). 2.30 - A review on applications of infrared heating for food processing in comparison to other industries. In K. Knoerzer, & K. Muthukumarappan (Eds.), *Innovative Food Processing Technologies* (pp. 431–455). Elsevier. https://doi.org/10.1016/B978-0-08-100596-5.22670-X.

Liu, X., Le Bourvellec, C., & Renard, C. M. (2020). Interactions between cell wall polysaccharides and polyphenols: Effect of molecular internal structure. *Comprehensive Reviews in Food Science and Food Safety, 19*(6), 3574–3617. https://doi.org/10.1111/1541-4337.12632

Liu, Y., Tian, J., Hu, B., Yu, P., & Fan, L. (2021). Relationship between crust characteristics and oil uptake of potato strips with hot-air pre-drying during frying process. *Food chemistry, 360*, Article 130045. https://doi.org/10.1016/j.foodchem.2021.130045. Article.

Luna-Zapién, E. A., Zegbe, J. A., Meza-Velázquez, J. A., & Minjares-Fuentes, R. (2023). Cactus pear (Opuntia spp.) mucilage and its application as food additive: An overview. *Revista Fitotecnia Mexicana, 46*(1), 51–61. https://doi.org/10.35196/rfm.2023.1.51

Martinez-Molina, W., Torres-Acosta, A., Hernández-Leos, R., Alonso-Guzman, E., Mendoza-Pérez, I., & Martinez-Peña, I. (2016). The inhibitive properties of Nopal slime on the corrosion of steel in chloride-contaminated mortar. *Anti-Corrosion Methods and Materials, 63*(1), 65–71. https://doi.org/10.1108/ACMM-05-2014-1381

Maskan, M. (2001). Drying, shrinkage and rehydration characteristics of kiwifruits during hot air and microwave drying. *Journal of Food Engineering, 48*(2), 177–182. https://doi.org/10.1016/S0260-8774(00)00155-2

McDougall, G. J., Kulkarni, N. N., & Stewart, D. (2009). Berry polyphenols inhibit pancreatic lipase activity *in vitro*. *Food Chemistry, 115*(1), 193–199. https://doi.org/10.1016/j.foodchem.2008.11.093

Medina-Torres, L., Gallegos-Infante, J., Gonzalez-Laredo, R., & Rocha-Guzman, N. (2008). Drying kinetics of nopal (*Opuntia ficus-indica*) using three different methods and their effect on their mechanical properties. *LWT-Food Science and Technology, 41*(7), 1183–1188. https://doi.org/10.1016/j.lwt.2007.07.016

Moses, J., Norton, T., Alagusundaram, K., & Tiwari, B. (2014). Novel drying techniques for the food industry. *Food Engineering Reviews, 6*, 43–55. https://doi.org/10.1007/s12393-014-9078-7

Motevali, A., Minaei, S., Khoshtaghaza, M. H., & Amirnejat, H. (2011). Comparison of energy consumption and specific energy requirements of different methods for drying mushroom slices. *Energy, 36*(11), 6433–6441. https://doi.org/10.1016/j.energy.2011.09.024

Neter, J., Wasserman, W., & Kutner, M. H. (1983). *Applied linear regression models*. Richard D. Irwin.

Nowak, D., & Lewicki, P. P. (2004). Infrared drying of apple slices. *Innovative Food Science & Emerging Technologies, 5*(3), 353–360. https://doi.org/10.1016/j.ifset.2004.03.003

Ortiz-Rodríguez, N., Condorí, M., Durán, G., & García-Valladares, O. (2022). Solar drying Technologies: A review and future research directions with a focus on agroindustrial applications in medium and large scale. *Applied Thermal Engineering, 215*, Article 118993. https://doi.org/10.1016/j.applthermaleng.2022.118993. Article.

Ortiz-Rodríguez, N., Marín-Camacho, J., Llamas-González, A., & García-Valladares, O. (2021). Drying kinetics of natural rubber sheets under two solar thermal drying systems. *Renewable Energy, 165*, 438–454. https://doi.org/10.1016/j.renene.2020.11.035

Ouhammou, M., Nabil, B., Hidar, N., Ouaabou, R., Bouchdoug, M., Jaouad, A., & Mahrouz, M. (2021). Chemical activation of the skin of prickly pear fruits and cladode *Opuntia megacantha*: Treatment of textile liquid discharges. *South African Journal of Chemical Engineering, 37*, 118–126. https://doi.org/10.1016/j.sajce.2021.04.006

Pan, Z., & McHugh, T. (2006). *Novel Infrared dry-Blanching (IDB), Infrared Blanching and Infrared Drying Technologies for food Processing*.

Ramírez-Arpide, F. R., Espinosa-Solares, T., Gallegos-Vázquez, C., & Santoyo-Cortés, V. H. (2019). Bioenergy production from nopal cladodes and dairy cow manure on a farm-scale level: Challenges for its economic feasibility in Mexico. *Renewable Energy, 142*, 383–392. https://doi.org/10.1016/j.renene.2019.04.093

Ramírez-Moreno, E., Córdoba-Díaz, D., de Cortes Sánchez-Mata, M., Díez-Marqués, C., & Goñi, I. (2013). Effect of boiling on nutritional, antioxidant and physicochemical characteristics in cladodes (*Opuntia ficus indica*). *LWT-Food Science and Technology, 51*(1), 296–302. https://doi.org/10.1016/j.lwt.2012.10.005

Rastogi, N. K. (2021). 2.31 - Infrared heating in drying operations. In K. Knoerzer, & K. Muthukumarappan (Eds.), *Innovative food processing technologies* (pp. 456–476). Elsevier. https://doi.org/10.1016/B978-0-08-100596-5.22671-1.

Salarikia, A., Miraei Ashtiani, S. H., & Golzarian, M. R. (2017). Comparison of drying characteristics and quality of peppermint leaves using different drying methods. *Journal of Food Processing and Preservation, 41*(3), Article e12930. https://doi.org/10.1111/jfpp.12930. Article.

Sánchez, C., Baranda, A. B., & de Marañón, I. M. (2014). The effect of high pressure and high temperature processing on carotenoids and chlorophylls content in some vegetables. *Food Chemistry, 163*, 37–45. https://doi.org/10.1016/j.foodchem.2014.04.041

Sarpong, F., Zhou, C., Bai, J., Amenorfe, L. P., Golly, M. K., & Ma, H. (2019). Modeling of drying and ameliorative effects of relative humidity (RH) against β-carotene degradation and color of carrot (*Daucus carota* var.) slices. *Food Science and Biotechnology, 28*(1), 75–85. https://doi.org/10.1007/s10068-018-0457-3

Saura-Calixto, F., Goñi, I., Bravo, L., & Mañas, E. (1993). Resistant starch in foods: Modified method for dietary fiber residues. *Journal of Food Science, 58*(3), 642–643. https://doi.org/10.1111/j.1365-2621.1993.tb04346.x

Shi, J., Pan, Z., McHugh, T. H., Wood, D., Hirschberg, E., & Olson, D. (2008). Drying and quality characteristics of fresh and sugar-infused blueberries dried with infrared radiation heating. *LWT-Food Science and Technology, 41*(10), 1962–1972. https://doi.org/10.1016/j.lwt.2008.01.003

Si, X., Chen, Q., Bi, J., Yi, J., Zhou, L., & Wu, X. (2016). Infrared radiation and microwave vacuum combined drying kinetics and quality of raspberry. *Journal of Food Process Engineering, 39*(4), 377–390. https://doi.org/10.1111/jfpe.12230

Tan, S. P., Vuong, Q. V., Stathopoulos, C. E., Parks, S. E., & Roach, P. D. (2014). Optimized aqueous extraction of saponins from bitter melon for production of a saponin-enriched bitter melon powder. *Journal of Food Science, 79*(7), E1372–E1381. https://doi.org/10.1111/1750-3841.12514

Tello-Ireland, C., Lemus-Mondaca, R., Vega-Gálvez, A., López, J., & Di Scala, K. (2011). Influence of hot-air temperature on drying kinetics, functional properties, colour, phycobiliproteins, antioxidant capacity, texture and agar yield of alga Gracilaria chilensis. *LWT-Food Science and Technology, 44*(10), 2112–2118. https://doi.org/10.1016/j.lwt.2011.06.008

Torres-Acosta, A. A., & Díaz-Cruz, L. A. (2020). Concrete durability enhancement from nopal (*Opuntia ficus-indica*) additions. *Construction and Building Materials, 243*, Article 118170. https://doi.org/10.1016/j.conbuildmat.2020.118170. Article.

Touil, A., Chemkhi, S., & Zagrouba, F. (2010). Modelling of the drying kinetics of Opuntia ficus indica fruits and cladodes. *International Journal of Food Engineering, 6*(2). https://doi.org/10.2202/1556-3758.1589

Tsotsas, E., & Mujumdar, A. S. (2011). *Modern drying technology, volume 4: Energy savings, 4*. John Wiley & Sons.

Ullah, I., Yin, T., Xiong, S., Zhang, J., Din, Z.-u., & Zhang, M. (2017). Structural characteristics and physicochemical properties of okara (soybean residue) insoluble dietary fiber modified by high-energy wet media milling. *LWT-Food Science and Technology, 82*, 15–22. https://doi.org/10.1016/j.lwt.2017.04.014

Wu, B., Ma, Y., Guo, X., Guo, Y., Qiu, C., Gao, K., Ma, H., & Pan, Z. (2023). Catalytic infrared blanching and drying of carrot slices with different thicknesses: Effects on surface dynamic crusting and quality characterization. *Innovative Food Science & Emerging Technologies, 88*, Article 103444. https://doi.org/10.1016/j.ifset.2023.103444. Article.

Xu, B. J., & Chang, S. K. (2007). A comparative study on phenolic profiles and antioxidant activities of legumes as affected by extraction solvents. *Journal of Food Science, 72*(2), S159–S166. https://doi.org/10.1111/j.1750-3841.2006.00260.x

Yang, M., Hou, C.-Y., Hsu, H.-Y., Hazeena, S. H., Santoso, S. P., Yu, C.-C., Chang, C.-K., Gavahian, M., & Hsieh, C.-W. (2022). Enhancing bioactive saponin content of raphanus sativus extract by thermal processing at various conditions. *Molecules (Basel, Switzerland), 27*(23), Article 8125. https://doi.org/10.3390/molecules27238125. Article.

Zawawi, N. A. F., Hazmi, N. A. M., How, M. S., Kantono, K., Silva, F. V., & Sulaiman, A. (2022). Thermal, high pressure, and ultrasound inactivation of various fruit cultivars' polyphenol oxidase: Kinetic inactivation models and estimation of

treatment energy requirement. *Applied Sciences, 12*(4), Article 1864. https://doi.org/10.3390/app12041864. Article.

Zhang, M., Chen, H., Mujumdar, A. S., Tang, J., Miao, S., & Wang, Y. (2017). Recent developments in high-quality drying of vegetables, fruits, and aquatic products. *Critical Reviews in Food Science and Nutrition, 57*(6), 1239–1255. https://doi.org/10.1080/10408398.2014.979280

Zhao, S., Pan, Z., Azarakhsh, N., Ramaswamy, H. S., Duan, H., & Wang, C. (2024). Effects of high-pressure processing on the physicochemical and adsorption properties, structural characteristics, and dietary fiber content of kelp (Laminaria japonica). *Current Research in Food Science, 8*, Article 100671. https://doi.org/10.1016/j.crfs.2023.100671. Article.